Research Article | Vol. 9, No. 8 / 1 August 2019 / Optical Materials Express 3432
Optical Materials EXPRESS

Fabrication and measurement of 3D printed retroreflective fibers

MICHAEL GHEBREBRHAN,[1,*] GABRIEL Z. J. LOKE,[2] AND YOEL FINK[2]

[1] U.S.Army Combat Capabilities Development Command Soldier Center, 10 General Greene Avenue, Natick, MA 01760, USA
[2] Department of Materials Science and Engineering, Massachusetts Institute of Technology, 77 Massachusetts Avenue, Cambridge, MA 02139, USA
[*] michael.ghebrebrhan2.civ@mail.mil

Abstract: Additive manufacturing enables new fiber preform geometries to be built that were either impossible or extremely difficult with traditional subtractive manufacturing methods. Additionally fiber thermal drawing is undergoing an explosion of interest due to new materials and fiber functions. We fabricate a retroreflective fiber that possesses a complex cross-section and material combination not achievable with other textile fiber fabrication methods such melt extrusion. This is the first such 3D-printing-derived fiber to demonstrate optical scattering properties with a non-circular, non-convex cross-section.

1. Introduction

Thermal drawing has recently undergone a resurgence of interest in producing sub-millimeter multifunctional and multimaterial fibers [1–3]. Originally developed for drawing silica glass fiber, it was the introduction of chalcogenide glasses to produce a cylindrical, 1D Bragg stack fiber that initiated the current level of interest [1]. Fibers with polymers, metals [4,5], semiconductors [6], elastomers [7], etc. have been co-drawn. These fibers up until recently have been drawn from preforms constructed through a "stack-and-press" or "roll-up" method where the preform components are stacked and then placed under heat and pressure to consolidate the stack into a single monolithic preform. The "roll-up" method has sheets of material stacked, rolled, and then consolidated with heat and pressure. Additive manufacturing has recently been used to construct fiber preforms [8,9]. Additive manufacturing, or 3D printing, builds objects by depositing material just where it is needed. Extruded filament layer-by-layer deposition, commonly known as fused filament fabrication, is a widely utilized technique for additive manufacturing, in which complex geometries with cavities, non-convex cross-sections and multiple materials can be built. 3D printing thus can easily deal with unusual cavities or complex cross-sections that would be very time-consuming to mill or too expensive to create a mold for it. Overcoming these challenges would enable new fiber functionalities derived from complex preform geometries.

Here we develop and fabricate a retroreflective fiber preform via 3D printing. The preform, illustrated in Fig. 1, has both polymer and metal. This fiber is designed to retroreflect light, i.e., the angle of reflection is the negative of the angle of incidence. Glass beads on a reflective surface are a familiar example of a retroreflective surface. To maximize retroreflectivity, the polymer's refractive index should be close to 1.9. At that index, a cylinder or sphere will refract light towards the intersection of the optical axis and back surface. Intrinsic retroreflectivity within the fiber would be a useful property as it allows other critical aspects of the textile (such as appearance and feel) it is woven into to be retained. In addition this design possesses a complex non-convex cross-section with multiple materials. A retroreflective fiber with an earlier design was developed and drawn via melt-extrusion [10]. Simultaneously a new design was proposed that would be more robust to imperfections. Melt extrusion is the process where a thermoplastic

#369054 https://doi.org/10.1364/OME.9.003432
Journal © 2019 Received 10 Jun 2019; revised 8 Jul 2019; accepted 14 Jul 2019; published 22 Jul 2019

Optical Materials EXPRESS

is brought to the molten state and then forced through an extrusion die. While it is the primary method for producing textile fibers, its downside is that the high temperatures greatly reduce the polymer viscosity which allow cross-sectional deformation to occur and destroy delicate features. Another issue with melt extrusion is coextruding metal and polymer. In the previous design, cross-sectional deformation occurred and the inner corner angles deviated from 90° in an uncontrolled manner [10]. Here, with a more robust structural design and by harnessing the ability of thermal drawing to better control polymer viscosity, we are able to co-draw metal and polymer to form a retroreflective fiber with its performance aided by its distinct polymeric structural shape and the high reflection properties of the metal.

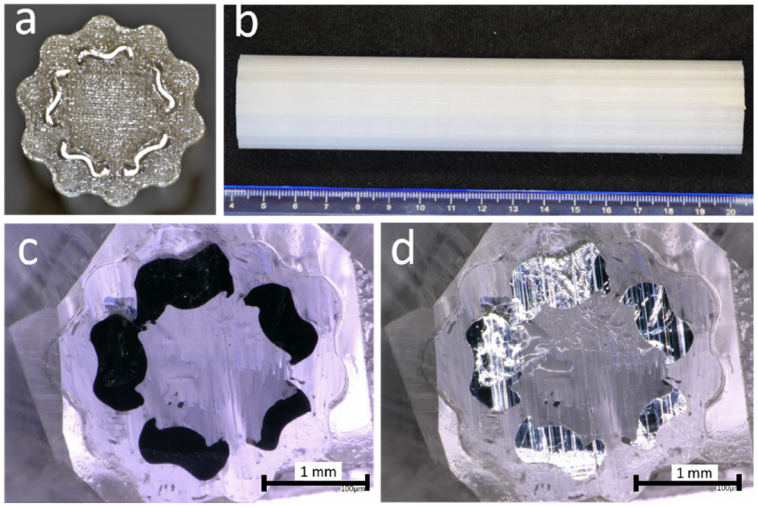

Fig. 1. a) Top view of the 3D printed polycarbonate (PC) preform with five indium strips in the channels. The outer cross-section of the preform contains a curvy serpentine outline. b) Side view of same preform. c) Epoxy-embedded drawn fiber under a microscope (transmitted light image). d) Same sample but reflected light. Both images in c and d illustrate the same curvy serpentine indium architecture as that constructed in the preform

The paper is organized as follows: we briefly describe the operation of the fiber design. Next we describe the fabrication of the preforms and fiber, including both the 3D printing parameters and fiber draw conditions. We conclude with retroreflection measurements of drawn fiber and future effort to obtain higher retroreflection.

2. Fabrication of preform and fiber

2.1. Preform printing

The preforms are constructed from polycarbonate (PC) and indium. For thermal drawing it would be ideal for both to have melting points or glass transition temperatures near each other. While the inner material, indium in our case, can have a melting point much below the cladding material's glass transition temperature [11], in cases where the cladding is thin and the denser metallic material is thick it is advantageous to have transition temperatures close to one another to prevent preform deformation caused by pooling of the molten metal. Polycarbonate's glass transition temperature is 160 °C [12] while indium's melting temperature is 156 °C [13]. Moreover, for retroreflectivity the polymer must be transparent and possess a high elongational viscosity to resist deformation during drawing. Indium is very ductile at room temperatures which ensures drawn fiber remains flexible at room temperature. The preforms have a diameter of 3 cm and height of 16 cm (Fig. 1). The channels are only 6 cm deep; the bottom 10 cm of the preform is

Optical Materials EXPRESS

solid which helps with fiber drawing as explained below. We print the preforms with a Stratasys Fortus 450MC printer which utilizes fused filament fabrication [14]. To ensure that the preforms are tough enough to withstand the draw tension the raster thickness, which controls how wide an extruded filament is laid down, was kept at 0.020 in (0.508 mm). The in-fill percent, which controls the fill fraction of polymer, is kept at the highest setting allowed by the machine. Prior attempts to increase the in-fill percent by printing with a smaller raster thickness, 0.007 in (0.178 mm), resulted in failed drawing. The toolpath of the printer nozzle is another important aspect to consider to ensure minimal deformation occurs. Because indium is much more dense than PC (ρ_{PC} = 1.2 g · cm^{-3} and ρ_{In} = 7.31 g · cm^{-3}) and placed near the outer surface, the preform must be stiff enough at its walls to resist deformation during drawing. Hence a print path that traces multiple concentric paths should be used to counteract the outward hydrostatic pressure from the liquid indium for preserving the cross-section and preventing pooling (lumping) of indium in the draw furnace. In Fig. 2 we trace the development of the cross-section to a final form that yielded fiber. Going from left to right, the preform's outer ring was made progressively stronger and the volume of the channels was made progressively smaller. Reducing the channel volume reduces the hydrostatic stress exerted by liquid indium on the outer ring during drawing. Previous fibers utilizing indium and other polymers encountered similar problems but cladded the fiber with Zeonex and PMMA [11,15]. Reference [4] utilized a clever strategy of incorporating a polymer with a lower glass transition temperature in the core to ensure a similar viscosity on both sides of the indium layer. We note in both cases the cross-sections and material interfaces were circular. Bridges connecting the outer ring to the PC core were increased in number and printed such that voids were minimized.

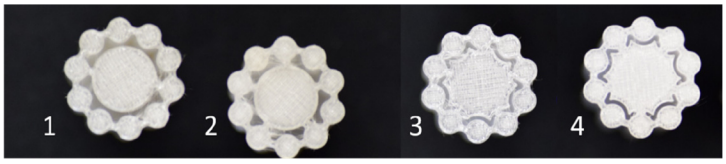

Fig. 2. Evolution of 3D printed preform cross-section: 1) two bridges to connect outer ring to inner PC core, 2) five bridges to reinforce outer ring, 3) similar to 2 but reduction of channel volume to reduce indium volume and outwards stress during draw, 4) similar to 3 but with thicker bridges for further reinforcement.

Indium foil of thickness 0.5 mm was inserted as thin strips. The channels need to be fully filled as any gaps would create unbalanced lateral stresses that deform the fiber's cross-section and create segments where not all channels are filled simultaneously. In addition, indium and PC have a high surface energy and indium does not wet PC's surface. So melt-casting indium within the preform channels tends not to backfill narrow unfilled channels.

2.2. Fiber drawing

Within the furnace during thermal drawing, the critical transition region from preform to fiber is known as the neck-down region. The neck-down region is quite short, all of the action occurs in just a few centimeters. Heat and draw tension is applied to elongate the viscous preform section into a fiber. To prevent pooling of indium, we keep the dwell time and maximum temperature in the furnace as low as possible. However because the preform is 3D printed, its strength is not as high as a solid rod, thus its desired viscosity when drawing must be lower than that of a solid preform. This is accomplished by building a preform with a long solid bottom which allows us to accelerate bait-off (i.e., the initial drop of preform attached to fiber) by higher temperatures, while the temperature of the retroreflective section does not increase beyond the T_g of PC. (Referring to Fig. 1(b), the first 10 cm of the preform is solid, while the last 6 cm has the channels with

Optical Materials EXPRESS

indium.) Once bait-off occurs the furnace temperatures are immediately dropped, giving the preform time to reach a new, lower draw temperature while the indium-filled section is still far from the neck-down region. We note that prior to drawing, the preforms are dried in a vacuum oven for a week at around 110 °C to drive off any residual moisture.

For drawing we utilize a three-zone furnace. The polymer's viscosity-temperature curve informs us the optimal drawing temperature. The furnace's middle zone is initially set at 250 °C for bait-off. Once bait-off has occurred, the temperature is immediately ramped down to 230 °C. If the temperature is too high, the polymer's viscosity is too low and the cross-section will deform under the stress of the indium's weight. If the temperature is too low, the preform cannot elongate and snaps apart. The temperature of the top zone is set at 150 °C until bait-off and then reduced to 130 °C. The bottom zone temperature is set at 110 °C until bait-off and then reduced to 90 °C. Table 1 organizes the draw conditions before and after bait-off. Table 1 lists the furnace temperatures and draw speeds before and after bait-off.

Table 1. Draw conditions

	Before bait-off	After bait-off
Top zone temperature (°C)	150	130
Middle zone temperature (°C)	250	230
Bottom zone temperature (°C)	110	90
Draw speed (m/min)	0.376	0.376
Feed speed (mm/min)	0.250	0.250

The abrupt change in cross-section, from solid PC to PC with indium, creates a perturbation to the steady-state. The draw tension is acting on a cross-section with less PC. (The indium strips contributes almost nothing to draw tension as it is a liquid in the neck-down region.) As the tension is fixed, the stress must increase. And since the indium is in the molten phase, it can pool at the bottom of its channel, bulging the fiber cross-section. Eventually, the stresses approach the steady-state and the fiber diameter converges to $d_{preform}\sqrt{v_{feed}/v_{draw}}$. The second effect could be mitigated by consolidating the preform before filling with indium or using a solid preform with milled channels.

From Fig. 1c and 1d tiny voids are visible within the fiber cross-section. These originate from the spaces between filaments in successive layers. They will degrade optical performance if in the outer ring. However, within the voids, the normal incidence reflectance at the polymer-air interface is 5.1% so the effect isn't too noticeable.

3. Optical measurements

A section of the fiber with all five channels filled was taken and examined for retroreflection (Fig. 1(c) and (d)). We use goniometer stage with an Ocean Optics HL-200 tungsten halogen light source connected to an Ocean Optics Reflection/Backscattering fiber optic probe. Light was focused on a spot along the fiber. The retroreflected light intensity was recorded with an Ocean Optics SD 2000 spectrometer. As our figure of merit we calculate the amount of light retroreflected by a single fiber relative to that of a white reflecting standard. Both are then scaled by the intercepted area. This yields a rescaled relative retroreflection ratio (RRR). Across the visible spectrum we obtain a rescaled RRR of roughly 260 (Fig. 3). We measure in six locations along the fiber axis and each time rotating it axially. We take a simple average to account for variations in the fiber's cross-section. Prior work with gold-coated retroreflective fibers demonstrated a rescaled RRR of 250—300 [10]. Simulations of a single retroreflecting fiber using the index of PC produce a RRR of about 269, which is slightly greater than the value obtained from experiments (Fig. 4). While deformation is evident in the fiber cross-section in

Optical Materials EXPRESS

Fig. 1c and 1d, we note that the critical features for retroreflectivity, the air-PC interface and outermost PC-indium interface have only slight deformation. This design is robust to slight deformations of the outer ring components [10]. Second, while the bridges negatively impact the RRR, it is mitigated by the fact that some light which strikes an indium-PC interface is reflected across the bridge to another indium-PC interface resulting in a 180° reversal of the incident light.

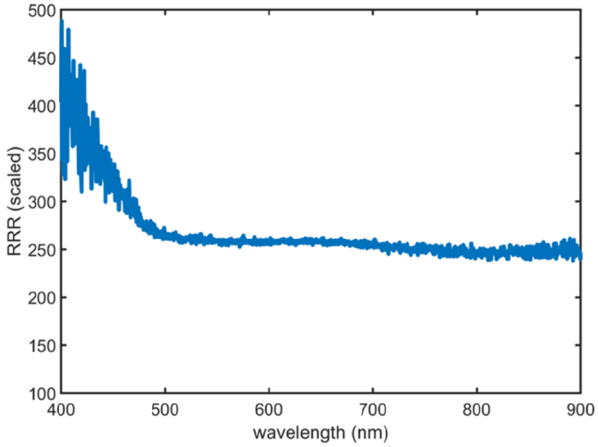

Fig. 3. Measured RRR of a single 3D-printed-derived retroreflective fiber across the visible spectrum.

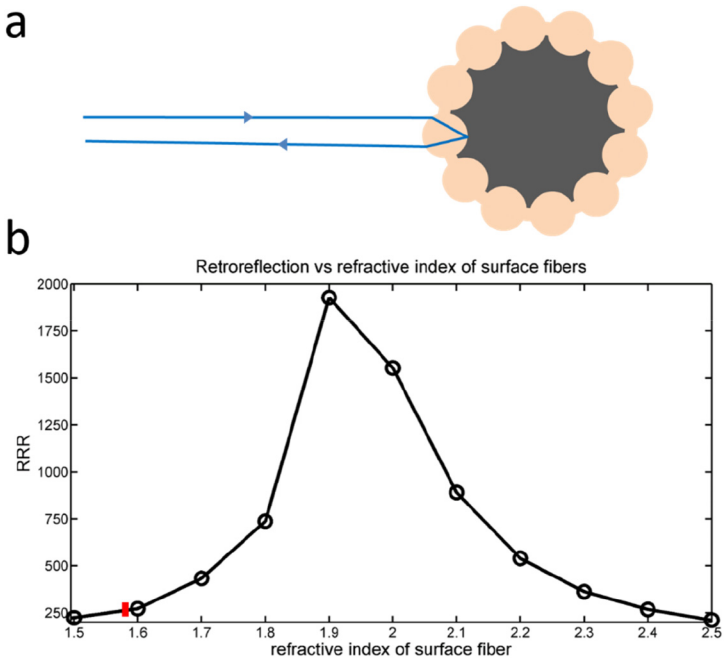

Fig. 4. a) Ray-trace illustrating retro-reflection. b) RRR versus refractive index of outer ring. The red line indicates our fiber (n = 1.58, RRR = 260). The peak RRR value occurs for a refractive index just over 1.9.

Optical Materials EXPRESS

By increasing the refractive index to n = 1.9, simulations suggest that the RRR can be as high as 2000 (Fig. 4). Polyetherimide has a refractive index of 1.68 but certain grades are not as transparent as PC [16]. Sulfur-containing polymers have demonstrated indices up to 1.80 [17]. A novel mixture of chalcogenide glasses with sulfur-containing polymer (dubbed "CHIPs") have produced samples with indices over 1.8 though attenuation below 700 nm becomes unacceptably high [18]. Using a polymer with n = 1.82 we expect a RRR of 800 to be attainable which is almost as good as metallized retroreflective glass beads. Of course, issues regarding thermal processing and optical clarity must be addressed.

4. Conclusions

In this paper we have demonstrated a novel fiber created with additive manufacturing. Despite being built by filament layer-by-layer, the interlayer fusion is strong enough to withstand the pulling tension during thermal drawing. However the voids created by neighboring filaments during 3D printing do not completely close and degrade the optical performance by creating scattering centers and deformation in the neck-down region. These voids can be eliminated by consolidating the preform above PC's glass transition temperature or modifying the print parameters such as raster thickness and in-fill percent.

Complex cross-section preforms are easily attainable with additive manufacturing and future efforts will explore the addition of multiple materials.

Funding

National Science Foundation (NSF) (DMR-1419807); Army Research Office (ARO) (W911NF-13-D-0001); Natick Soldier Research, Development and Engineering Center (NSRDEC).

Acknowledgements

M. G. would like to thank M. Hurley for printing the preforms, B. A. Welsh for useful discussions regarding melt extrusion of complex cross-sections, and M. Rein for initial assistance and insight into thermal drawing. G. L. was supported in part by the National Science Foundation under the Materials Research Science and Engineering Center (MRSEC) program (Award number DMR-1419807) and in part by the US Army Research Laboratory and the US Army Research Office through the Institute for Soldier Nanotechnologies, under contract number W911NF-13-D-0001. M. G. was supported in part by CCDC-SC Section 2363 funding.

References

1. S. D. Hart, G. R. Maskaly, B. Temelkuran, P. H. Prideaux, J. D. Joannopoulos, and Y. Fink, "External reflection from omnidirectional dielectric mirror fibers," Science **296**(5567), 510–513 (2002).
2. G. Tao, H. Ebendorff-Heidepriem, A. M. Stolyarov, S. Danto, J. V. Badding, Y. Fink, J. Ballato, and A. F. Abouraddy, "Infrared fibers," Adv. Opt. Photonics **7**(2), 379–458 (2015).
3. T. Khudiyev, C. Hou, A. M. Stolyarov, and Y. Fink, "Sub-micrometer surface-patterned ribbon fibers and textiles," Adv. Mater. **29**(22), 1605868 (2017).
4. A. Tuniz, R. Lwin, A. Argyros, S. C. Fleming, E. M. Pogson, E. Constable, R. A. Lewis, and B. T. Kuhlmey, "Stacked-and-drawn metamaterials with magnetic resonances in the terahertz range," Opt. Express **19**(17), 16480–16490 (2011).
5. M. Bayindir, F. Sorin, A. F. Abouraddy, J. Viens, S. D. Hart, J. D. Joannopoulos, and Y. Fink, "Metal-insulator-semiconductor," Nature **431**(7010), 826–829 (2004).
6. D. S. Deng, N. D. Orf, A. F. Abouraddy, A. M. Stolyarov, J. D. Joannopoulos, H. A. Stone, and Y. Fink, "In-fiber semiconductor filament arrays," Nano Lett. **8**(12), 4265–4269 (2008).
7. Y. Qu, T. Nguyen-Dang, A. G. Page, W. Yan, T. Das Gupta, G. M. Rotaru, R. M. Rossi, V. D. Favrod, N. Bartolomei, and F. Sorin, "Superelastic multimaterial electronic and photonic fibers and devices via thermal drawing," Adv. Mater. **30**(27), 1707251 (2018).
8. P. M. Toal Jr., L. J. Holmes, R. X. Rodriguez, and E. D. Wetzel, "Microstructured monofilament via thermal drawing of additively manufactured preforms," Addit. Manuf. **16**, 12–23 (2017).

Optical Materials EXPRESS

9. K. Cook, J. Canning, S. Leon-Saval, Z. Reid, M. A. Hossain, J.-E. Comatti, Y. Luo, and G.-D. Peng, "Air-structured optical fiber drawn from a 3D-printed preform," Opt. Lett. **40**(17), 3966–3969 (2015).
10. M. Ghebrebrhan, L. C. Hoke, F. J. Aranda, M. L. Hoey, D. M. Archambault, J. Perry, L. Belton, D. Ziegler, J. B. Carlson, and B. R. Kimball, "Design and fabrication of extruded retroreflective polymer fibers," Opt. Mater. Express **4**(12), 2656–2662 (2014).
11. J. G. Hayashi, S. Fleming, B. T. Kuhlmey, and A. Argyros, "Metal selection for wire array metamaterials for infrared frequencies," Opt. Express **23**(23), 29867–29881 (2015).
12. https://www.stratasys.com/materials/search/pc-iso
13. J. R. Rumble, ed., CRC Handbook of Chemistry and Physics, CRC Press/Taylor and Francis, Boca Raton, FL 99th Ed., accessed February 2019.
14. https://www.stratasys.com/ Accessed March 8th, 2019.
15. N. Singh, A. Tuniz, R. Lwin, S. Atakaramians, A. Argyros, S. C. Fleming, and B. T. Kuhlmey, "Fiber-drawn double split ring resonators in the terahertz range," Opt. Mater. Express **2**(9), 1254–1259 (2012).
16. H. R. Philipp, D. G. Le Grand, H. S. Cole, and Y. S. Liu, "The optical properties of a polyetherimide," Polym. Eng. Sci. **29**(22), 1574–1578 (1989).
17. J.-G. Liu and M. Ueda, "High refractive index polymers: fundamental research and practical applications," J. Mater. Chem. **19**(47), 8907–8919 (2009).
18. M. Babaeian, L. R. Diaz, S. Namnabat, T. S. Kleine, A. Azarm, J. Pyun, N. Peyghambarian, and R. A. Norwood, "Nonlinear optical properties of chalcogenide hybrid inorganic/organic polymers (CHIPs) using the Z-scan technique," Opt. Mater. Express **8**(9), 2510–2519 (2018).